Spin-orbit control of antiferromagnetic domains without a Zeeman coupling

Damaris Tartarotti Maimone (damaris.tartarotti-maimone@psi.ch)
Paul Scherrer Institut
Junying Shen
Paul Scherrer Institut https://orcid.org/0000-0002-8703-120X
Nicolas Gauthier
Institut Quantique and Department de Physique
Daniel Mazzone
Paul Scherrer Institut https://orcid.org/0000-0002-0421-0625
Markus Zolliker
Paul Scherrer Institut
Ruchika Yadav
Paul Scherrer Institut
Romain Sibille
Paul Scherrer Institut https://orcid.org/0000-0001-6360-7262
Dariusz Gawryluk
Paul Scherrer Institute https://orcid.org/0000-0003-4460-7106
Ekaterina Pomajkushina
Paul Scherrer Institute https://orcid.org/0000-0002-2446-3830
Stéphane Raymond
CEA-Grenoble https://orcid.org/0000-0002-5421-5061
Eric Ressouche
Univ. Grenoble Alpes, CEA https://orcid.org/0000-0001-6364-1890
Christof Niedermayer
Paul Scherrer Institute https://orcid.org/0000-0001-6508-8988
Gérard Lapertot
University Grenoble Alpes / CEA https://orcid.org/0000-0001-6023-478X
Jorge Gavilano
Paul Scherrer Institut
Marek Bartkowiak
Paul Scherrer Institut https://orcid.org/0000-0001-9866-2165
Michel Kenzelmann
Paul Scherrer Institute https://orcid.org/0000-0001-7913-4826

Article

Keywords:

Posted Date: December 21st, 2023

DOI: https://doi.org/10.21203/rs.3.rs-2629966/v1

Additional Declarations: (Not answered)

Spin-orbit control of antiferromagnetic domains without a Zeeman coupling

D. T. Maimone,[1,2] J. Shen,[1,3] N. Gauthier,[1,4] D. G. Mazzone,[5] M. Zolliker,[1] R. Yadav,[1] R. Sibille,[5] D. J. Gawryluk,[6] E. Pomjakushina,[6] S. Raymond,[7] E. Ressouche,[7] C. Niedermayer,[5] G. Lapertot,[8] J. L. Gavilano,[5] M. Bartkowiak,[1] and M. Kenzelmann[5,2]

[1]*Laboratory for Neutron and Muon Instrumentation, Paul Scherrer Institut, CH-5232 Villigen PSI, Switzerland*

[2]*Department of Physics, University of Basel, Basel, Switzerland*

[3]*Institute of High Energy Physics, Chinese Academy of Sciences, Beijing 100049, China Spallation Neutron Source Science Center, Dongguan 523803, China*

[4]*Institut Quantique and Département de Physique, Université de Sherbrooke, Sherbrooke, Québec J1K 2R1, Canada*

[5]*Laboratory for Neutron Scattering and Imaging, Paul Scherrer Institut, CH-5232 Villigen PSI, Switzerland*

[6]*Laboratory for Multiscale materials Experiments, Paul Scherrer Institut, CH-5232 Villigen PSI, Switzerland*

[7]*Univ. Grenoble Alpes, CEA, IRIG, MEM, MDN, 38000, Grenoble, France*

[8]*Univ. Grenoble Alpes, CEA, INP, IRIG, PHELIQS, 38000, Grenoble, France*

Encoding information in antiferromagnetic (AFM) domains is a promising solution for the ever growing demand in magnetic storage capacity. What fundamentally enables ultrahigh density AFM-based spintronics is the absence of unintentional crosstalk between different domain states due to vanishing stray fields[1]. However, the absence of macroscopic magnetization is detrimental to the manipulation and detection of AFM domains. Disentangling the merits and disadvantages of small stray fields seemed so far unattainable. In this work, we report evidence for a new AFM domain selection mechanism based on the anisotropy in the susceptibility not induced by Zeeman energy terms, but by the relative orientation of the external magnetic field to the two perpendicularly oriented k-domains only. As a result, the charge transport response is controlled by the rotation of the magnetic field. In particular, a pronounced new anisotropic magnetoresistance effect is found in the AFM phase of bulk materials $Nd_{1-x}Ce_x$ $CoIn_5$, due to differences in transport scattering rates for currents applied parallel and perpendicular to the spin-density wave modulation. Our results and the domain switching theory[2] indicate that this constitutes a new universal effect across multiband materials and thus provide a novel mechanism to control and detect AFM domains opening new perspectives for AFM sprintronics.

Antiferromagnetism is preponderant among magnetically ordered materials. This type of ordering, defined by an antiparallel alignment of elementary magnetic moments, assumes a multitude of variations[3,4], including collinear and non-collinear antiferromagnets, modulated structures such as spin-density waves (SDW) and antiferromagnetic spin glasses[4]. Yet, despite the fact that we explore antiferromagnetic ordering for almost a century, the fundamental mechanisms for controlling antiferromagnetic states among different types of domains and orders remain challenging[5,6]. Establishing control and detection of antiferromagnetic domains open new windows of opportunity for both fundamental research and applications[1,7].

In the era of information and data science, spintronics has become a topic of intense research, since it offers the possibility of obtaining non-volatility, reduced power consumption, increased data processing speed, and high density magnetic memories[8]. In this field, antiferromagnets have several advantages over ferromagnetic materials, as they possess ultrafast spin dynamics[1,9–13] and small or non-existent stray fields[1,7,12]. The terahertz control of the spin degree of freedom enables high speed data processing[12,13]. The absence of stray fields makes these materials robust against magnetic perturbations[1], offering the possibility of obtaining even higher density information storage when antiferromagnets are utilized in active components of spintronic devices. However, higher robustness has also meant that it has been more difficult to manipulate different binary states and detect them. The efficient manipulation[6] and detection[1,7] of AFM domains are among the most pressing problems to be solved.

Direct manipulation of AFM domains through the application of a strong magnetic field often relies on the Zeeman coupling term ($\boldsymbol{H} \cdot \boldsymbol{\mu}$, where $\boldsymbol{\mu}$ indicates the direction of the ordered moments) and therefore on the relative orientation between the applied field and the spin orientation. An example is found in elemental chromium, where a single magnetic domain (single k-domain) state in a transverse SDW can be obtained through the application of a sufficiently large field[14,15]. On the detection side, beyond utilizing optical and scattering techniques[16], probing domain states in the charge channel is essential for applications[7]. Charge-detection of different antiferromagnetic states in bulk materials, i.e. the AFM-based anisotropic magnetoresistance (AMR), often relies on electronic scattering on domain walls[17] or a change in the density of states near the Fermi level due to the opening of a gap-type antiferromagnetism (as in chromium[18,19]) or relativistic spin-orbit coupling[20,21]. In the latter, distinctive resistive states arise due to the anisotropy of the electronic structure when the AFM moments are aligned along different crystallographic directions[20]. In fact, most of the explored effects involve the spin orientation either in the manipulation or the detection of AFM states. However, in most cases, the outcome from each of the effects above trigger small readout signals that are incompatible with the scalability of devices[1,7,22]. Thus, new conceptual and experimental advancements on how to manipulate and detect AFM domains are required. Finding ways to decouple the spin orientation from magnetoelectronic phenomena could offer easier ways to manipulate and detect AFM domains.

In this context, we focus on a recent theoretically proposed mechanism suggested to occur in centrosymmetric multiband metals with large spin-orbit coupling (SOC)[2]. A spin susceptibility anisotropy was predicted to arise from interband spin-orbit coupling[2] in a similar manner to what is observed in non-centrosymmetric materials[23]. In the latter, Rashba-type interactions are of key importance for spintronics applications[7,24], because it introduces a non-trivial SOC which results in an anomalous anisotropic spin susceptibility[25]. Instead, in centrosymmetric materials, it is the multiband nature of the electronic structure which is responsible for such anisotropy, providing a mutual coupling between the AFM ordering vector and the field direction[2]. The theoretical model anticipates that, for a magnetic structure where several k-domains are allowed by the crystal structure, interband SOC gives rise to a static susceptibility $\chi(\boldsymbol{k}, \boldsymbol{H})$ that is largest either at $\boldsymbol{k} \parallel \boldsymbol{H}$ or $\boldsymbol{k} \perp \boldsymbol{H}$, for fields applied transversely to the moment direction[2]. Therefore, a rotation of the magnetic field direction in the plane perpendicular to the moments becomes a way to manipulate the AFM domains (see Fig.1(a) and (b)). The proposed mechanism is an intrinsic electronic effect present in antiferromagnetic materials that does not depend on a Zeeman term and has not been fully experimentally validated or explored yet.

Very recently, the emergence of itinerant antiferromagnetism has been observed in the large spin-orbit coupled multiband compounds $Nd_xCe_{1-x}CoIn_5$ with $x \leq 0.25$[26–28]. These compounds crystallize in the centrosymmetric tetragonal structure with space group $P4/mmm$[26]. The degeneracy of the tetragonal structure allows for two k-domains in the SDW phase, which are indeed confirmed[27]. The magnetic moments point along the tetragonal c-axis with an amplitude that is modulated along two orthogonal directions in the *ab-plane* (see Fig.1(a)). The superconducting state of the parent compound, $CeCoIn_5$, hosts a SDW with the same magnetic symmetry[29]. There, the population of k-domains completely switches upon rotation of the magnetic field within only $\sim 0.1^o$[29]. However, since the AFM phase in the pure compound is exclusively present in the zero-resistive state, magnetoresistive effects cannot be investigated. In addition, the origin of this phenomena is indistinguishable from scenarios where a coupling between magnetism and superconductivity[29,30] is essential. Antiferromagnetism detaching from the superconducting state under Nd substitution[27,31] allows us to fully explore the aforementioned proposed phenomenon.

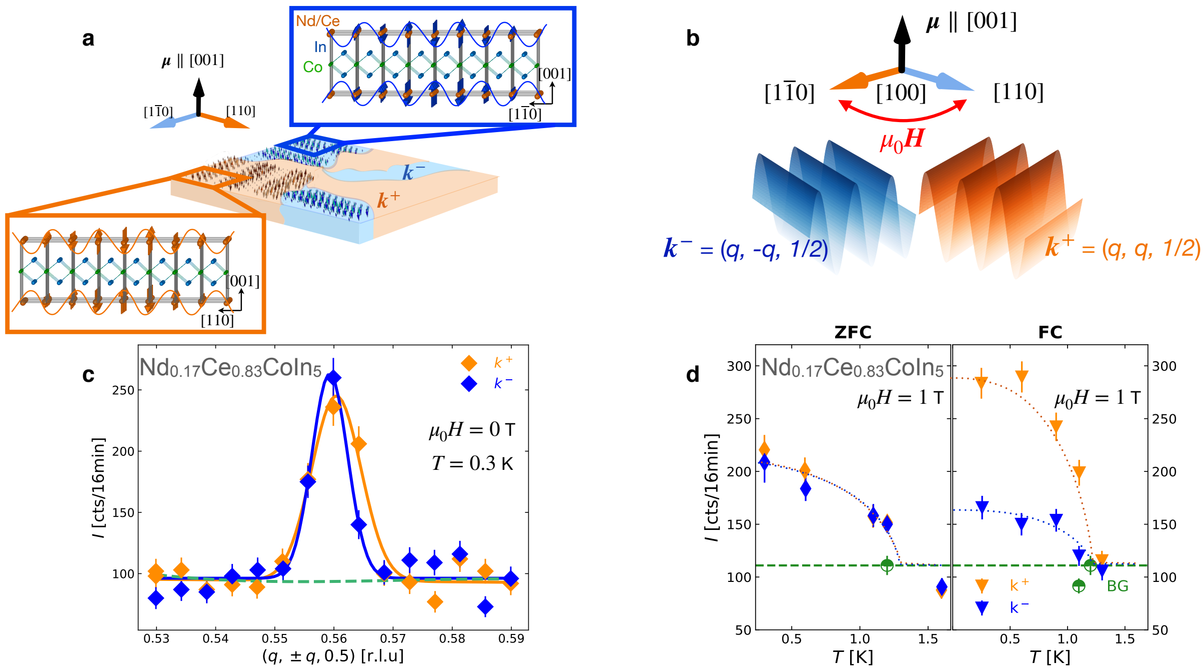

FIG. 1: **SDW domain switching:** **(a)** schematic diagram of the k-domains in the sample along with their amplitude modulated magnetic structures. The orange and blue arrows indicate the direction of the static magnetic moments ($\boldsymbol{\mu}$) pointing along the [001] direction and modulated with two orthogonal ordering vectors $\boldsymbol{k}^+$ and $\boldsymbol{k}^-$. The static moments are located on the rare earth site, indicated by the orange balls. Blue and green balls indicate the In and Co ions. **(b)** shows the $\boldsymbol{k}^+$ and $\boldsymbol{k}^-$ domains. As the field is rotated in the ab-plane across the [100] crystallographic direction, the SDW domains switch, favoring the domain whose modulation is most perpendicular to the field direction. **(c)** The scans display the diffracted neutron intensity in counts per 16 minutes along $(q, \pm q, 0.5)$ in (r.l.u.). **(d)** Temperature dependences of the magnetic Bragg peak intensities of the two magnetic domains measured at $\mu_0 H = 1$ T in zero field cooled (ZFC) and field cooled (FC) conditions.

The magnetic structures of $Nd_xCe_{1-x}CoIn_5$ spontaneously form two equally populated k-domains at zero magnetic field. The real space representation of the two k-domains is depicted in Fig.1(b). In reciprocal space, these two domains are described by two subsets of k-vectors forming an eightfold star (see Supplementary Information I). By mirror and translational symmetry operations, the eight vectors are attributed to either $\boldsymbol{k}^+$ or the $\boldsymbol{k}^-$ domains of form $(q, q, 0.5)$ and $(q, -q, 0.5)$, respectively. Fig.1(c) shows neutron diffraction data for wavevectors along the $(q, \pm q, 0.5)$ direction at low temperature and zero magnetic field for $Nd_{0.17}Ce_{0.83}CoIn_5$. Fig.1(d) displays the temperature dependence of the magnetic Bragg peak intensity at $\mu_0 H = 1$ T along the $[1\bar{1}0]$ direction in zero field (ZFC) and field cooled (FC) conditions. After zero field cooling, both domains reveal equal intensity below the Néel transition temperature T_N. Field cooling influences the domain formation, enhancing the intensity of the domain oriented most perpendicularly to the field direction, i.e. $\boldsymbol{k}^+$ for $\boldsymbol{H} \parallel [1\bar{1}0]$. Thus, the domain population can be controlled upon magnetic field without a Zeeman coupling.

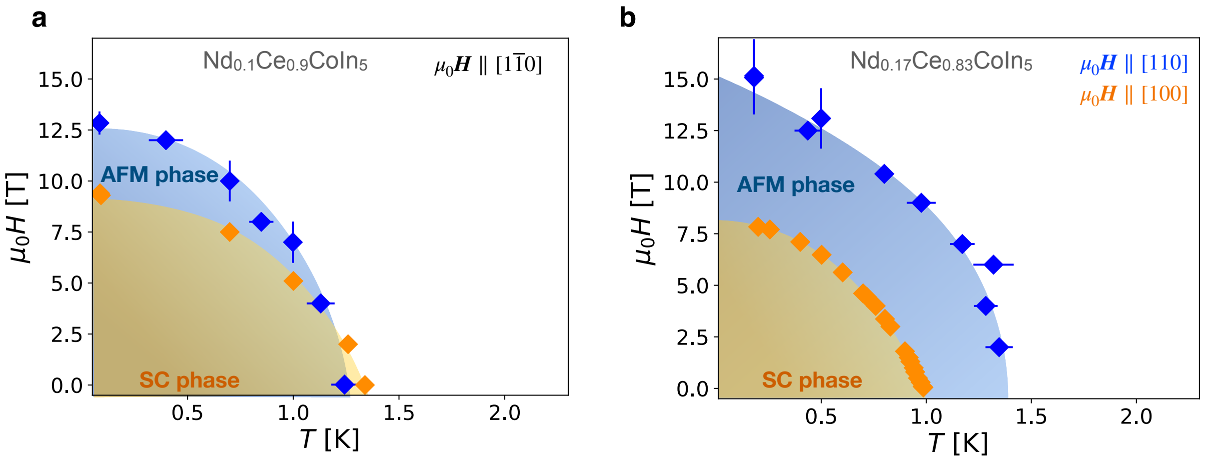

FIG. 2: **Magnetic order exceeds the superconducting phase.** HT-phase diagram of **(a)** $Nd_{0.1}Ce_{0.9}CoIn_5$ and **(b)** $Nd_{0.17}Ce_{0.83}CoIn_5$. , The magnetic phase boundaries were obtained from temperature and field scans of the Bragg reflection intensities. The superconducting phase boundaries were measured by electrical resistivity measurements.

Fig.2 displays the HT-phase diagrams of $Nd_{0.1}Ce_{0.9}CoIn_5$ and $Nd_{0.17}Ce_{0.83}CoIn_5$. In $Nd_{0.1}Ce_{0.9}CoIn_5$, magnetic order develops below a Néel temperature that is lower than the superconducting transition temperature T_c, but exists up to fields higher than the superconducting upper critical field H_{c2}. Upon further increasing the Nd content to 17%, superconductivity is completely enclosed by the magnetic phase. Thus, $Nd_xCe_{1-x}CoIn_5$ with $0.25 \geq x \geq 0.1$ is a regime where magnetic order is developed in the absence of superconductivity (see Supplementary Information II for $x = 0.25$ and also field dependences shown in Fig.3), providing an ideal test ground for theories assessing the SDW domain repopulation in the absence of a Zeeman coupling. This also allows us to clarify the role of superconductivity in this process.

For this purpose, we studied the evolution of the k-domain population as a function of magnetic field along the [1$\bar{1}$0] direction. Fig.3 displays the field dependences of magnetic Bragg peak intensities associated with the two domain states $\mathbf{k}^+$ and $\mathbf{k}^-$ for the 10%, 17% and 25% Nd substituted compounds. We find a field-induced domain imbalance of the k-domains, i.e. above a certain field, the intensity of the unfavored $\boldsymbol{k}^-$-domain drops to zero while the intensity of the $\boldsymbol{k}^+$ domain is increased. Remarkably, this happens in the absence of superconductivity (Fig.3(c) and (d)), and is indistinguishable from the domain selection in the superconducting state. Thus, our results establish that superconductivity is not necessary for the domain repopulation. The domain selection is not reversible with the removal of the magnetic field (see Supplementary information III). We note that the unfavored $\boldsymbol{k}^-$-domain is only formed when the system is reinitialized through zero field cooling or by in-situ rotation of the magnetic field direction. This

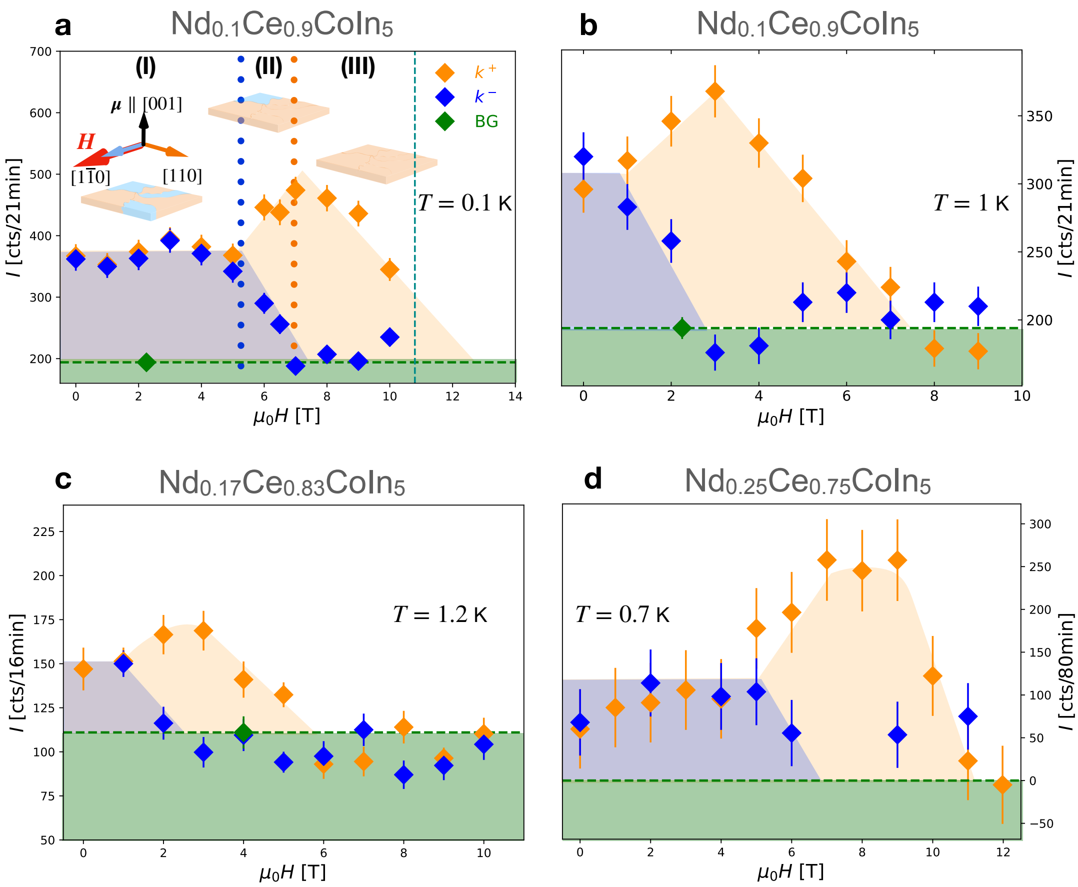

FIG. 3: **AFM domain selection in the superconducting and normal states:** magnetic Bragg peak intensity as a function of field along the [1$\bar{1}$0] direction at different temperatures for $Nd_{0.1}Ce_{0.9}CoIn_5$ (**(a)** and **(b)**), in the normal conducting state of $Nd_{0.17}Ce_{0.83}CoIn_5$ **(c)** and for the correlated metal $Nd_{0.25}Ce_{0.75}CoIn_5$ **(d)**. BG indicates the background, measured in the paramagnetic states of $Nd_xCe_{1-x}CoIn_5$. The rectangles displayed in **(a)** are a schematic view of the sample showing the evolution of the domain population. At low fields (regime I), both $\boldsymbol{k}^+$ and $\boldsymbol{k}^-$ domains are present with equal population. In regime II, a domain repopulation takes place, favoring the domain which is mostly perpendicular to the field direction, ie. $\boldsymbol{k}^+$. In regime III, a single $\boldsymbol{k}^+$ domain state is obtained. The vertical green line in **(a)** indicates the field where we have performed complementary electrical resistivity measurements (see Figs.4 and 5).

demonstrates that the AFM phase has a non-volatile memory effect. Note that non-volatility is a key asset for magnetic recording and it has been seldom reported in the literature for antiferromagnets[32], and antiferromagnetic metals in particular.

If the mutual dependence of the magnetic wavevector on the field direction indeed originates from an interband spin-orbit interaction, as suggested by theory, the effect should also be observable in transport properties. Therefore, we carried out experiments on the charge-detection of the SDW switching. Notably, we explored the magnetotransport effect of $Nd_{0.1}Ce_{0.9}CoIn_5$, for which a relatively large area of the SDW phase is observed in absence of superconductivity. Resistivity measurements were performed under a configuration where the electrical current was

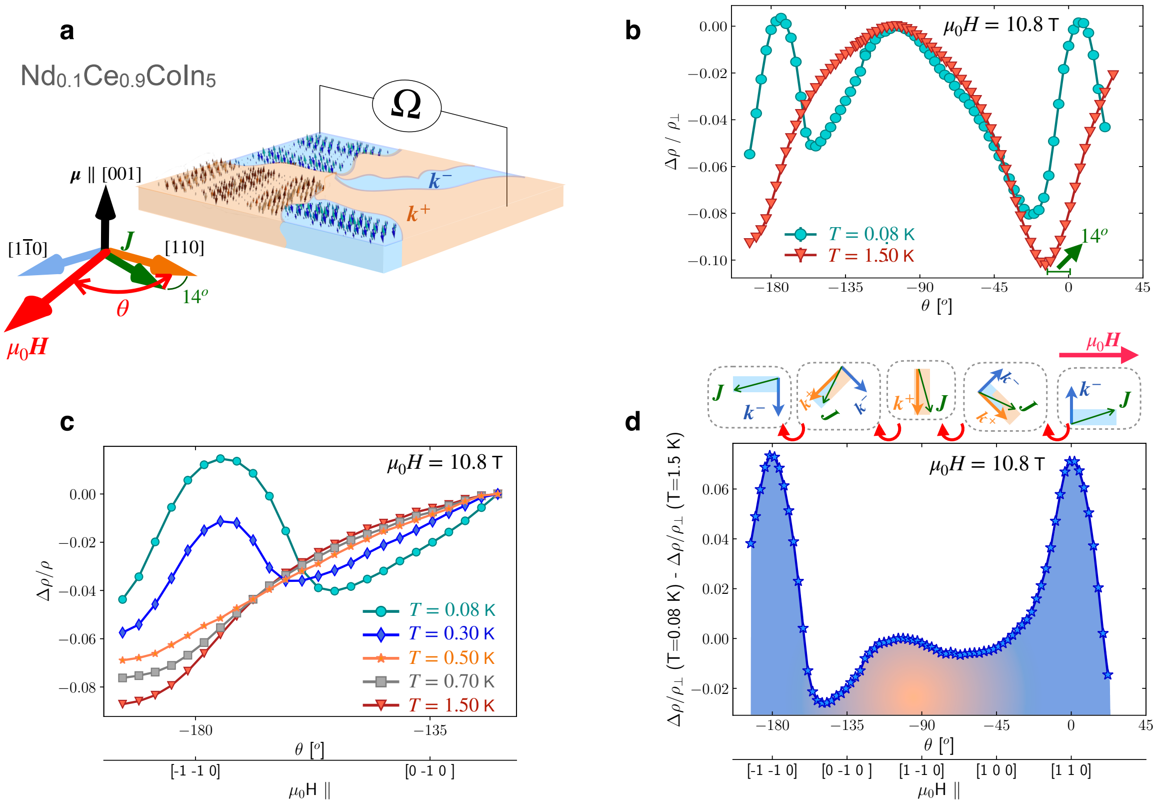

FIG. 4: **Anisotropic magnetoresistance in the AFM phase of $Nd_{0.1}Ce_{0.9}CoIn_5$: (a)** The electrical resistivity was measured along the $\boldsymbol{J} \parallel [110]$ direction with a misalignment of 14^o in the $ab-plane$. As the field is rotated across the [100] crystallographic direction, the SDW domains switch, thus changing the relative orientation between the current direction and the SDW modulation. **(b)** Angular dependence of resistivity normalized by the transverse resistivity for $T < T_N$ (green) and $T > T_N$ (red) at $\mu_0 H = 10.8$ T. The high temperature curve resembles the cyclotron effect observed up to temperatures higher than 20 K (Supplementary Information V). At low temperatures, an increased resistivity is found for $\boldsymbol{H} \parallel [110]$, i.e. when the current is perpendicular to the $\boldsymbol{k}^+$ or k^- domain. **(c)** Angular dependence of the electrical resistivity normalized by the value at $\theta \approx -120^o$ and $\mu_0 H = 10.8$ T for different temperatures. We observe a resistivity enhancement below the antiferromagnetic transition. **(d)** Angular dependence of the AFM AMR where the paramagnetic contribution has been subtracted. In the schematic diagram, $\boldsymbol{k}$ represents the ab-plane components of the two-domains.

intentionally misaligned 14^o to the [110] direction in the $ab-plane$. This allowed us to distinguish scenarios where the magnetoelectronic effect is purely related to the magnetic structure or to the relative orientation between the electrical current and the field. As the magnetic field is rotated, the SDW modulation alternates from being mostly perpendicular to being mostly parallel to the current direction (see Fig.4(a)). In Fig.4 (b), we depict the angular dependence of the magnetoresistance ratio defined as $\Delta\rho/\rho_\perp = [\rho(\theta) - \rho_\perp]/\rho_\perp$, where $\rho_\perp$ is the transverse magnetoresistance, i.e. the resistivity value when the current is applied perpendicularly to the magnetic field direction. The angular scans were obtained in zero field cooling conditions and the field was applied first close to the symmetrically equivalent $[0\bar{1}0]$ direction. Note that the two domains are degenerate for fields applied along [010] and [100], because $\boldsymbol{k}^+$ and $\boldsymbol{k}^-$ have equal components parallel to the field direction (see Supplementary Information I). Hence, these directions do not favor any domain and are called symmetrically equivalent. $\Delta\rho/\rho_\perp$ at $T = 1.5$ K> T_N displays a two-fold symmetry with a resistance minimum for $\boldsymbol{J} \parallel \boldsymbol{H}$ and a large magnetoresistance for $\boldsymbol{J} \perp \boldsymbol{H}$. This is due to the cyclotron effect and is expected for metals[33,34]. Under the application of a magnetic field, the charge carriers are subjected to a Lorentz force that modifies the electronic trajectories. When the current is applied perpendicularly to the field direction, the Lorentz force is maximal and a longer electronic path results in an increased resistance (see also Supplementary Information V). The similarity of the low and high temperature magnetoresistance anisotropy at field directions close to $\theta = -90^o$ indicate that the Lorentz force dominates the scattering process in this angular range. The low temperature anisotropic magnetoresistance (AMR) measured below T_N at $T \approx 80$ mK is superimposed on the high temperature data. We found an additional contribution to the resistivity for fields applied along the [±1 ±1 0] crystallographic directions. These peaks are present at temperatures below the AFM transition (see Fig.4(c)) and are directly related to the emergence of antiferromagnetism in $Nd_{0.1}Ce_{0.9}CoIn_5$ (see Fig.5).

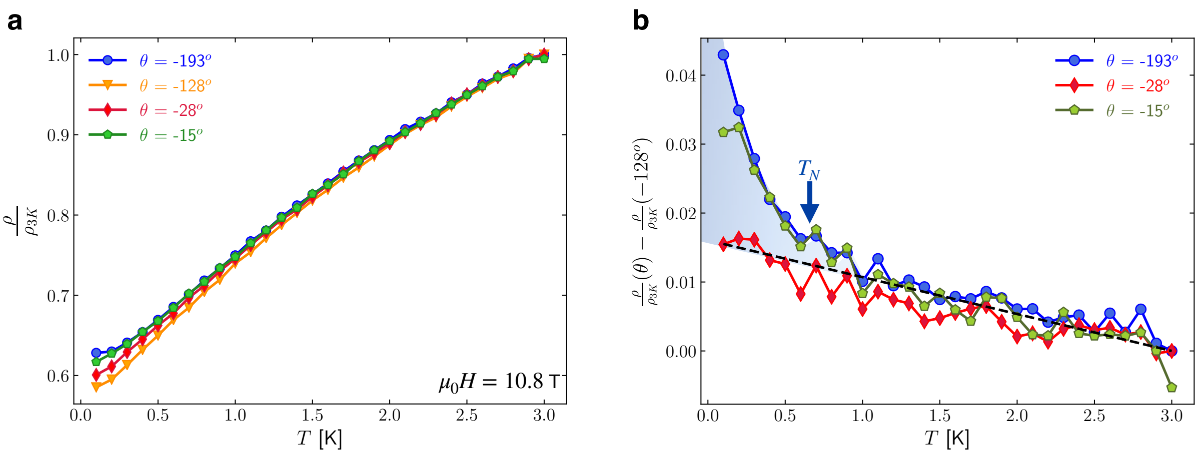

FIG. 5: **Transport in the AFM phase of $Nd_{0.1}Ce_{0.9}CoIn_5$: (a)** Temperature dependence of electrical resistivity inside the antiferromagnetic phase for different magnetic field orientations. **(b)** The difference of the normalized resistivities at various field orientations with respect to the normalized resistivity at $\theta = -128^o$ shows that additional anisotropic magnetoresistance develops only inside the antiferromagnetic phase. The background level is obtained via linear regression of all three resistivity curves at temperatures larger than 0.7 K and extrapolated to low temperatures.

Fig.5(a) displays the normalized resistivity as a function of temperature, where the normalization at $T = 3$ K integrates out the paramagnetic cyclotron effect. Fig.5(b) shows the difference between the normalized resistivities plotted in Fig.5(a) and the normalized resistivity at $\theta = -128^o$. Their subtraction $\rho(\theta) - \rho(\theta = -128^o)$ reveals the origin of the resistivity enhancement attributed to the peaks shown in Fig.4(b) and (c). Fig.5(b) provides evidence for a dramatic resistivity increase below the antiferromagnetic transition, conclusively connecting the exotic AMR with the emergence of AFM.

The emergence of this resistivity enhancement is a signature of the antiferromagnetic state, but it also correlates with the domain switching effect. Fig.4(d) shows the two-fold AMR signal that arises inside the AFM phase. Here, the paramagnetic contribution has been subtracted. We observe a higher resistivity when the current is oriented perpendicular to the modulation of one k-domain, i.e. where $\boldsymbol{k}^-$ is energetically favorable. A more conductive state is found when $\boldsymbol{k}^+$, which has modulation roughly parallel to $\boldsymbol{J}$, is favored by the field orientation. This is intrinsic AMR is ruled by the angle between the electric current direction and the ordering vector, rather than the orientation between the current and the magnetic field direction. In the latter case, one would expect the maximum in AMR at a slightly different angle due to the small misalignment between the current direction and the [110] crystallographic orientation. In fact, the peak in the AMR. for the ordered state would coincide with the minimum of the paramagnetic AMR, which is not what we observe. We can also exclude an enhanced scattering due to domain walls because the largest number of domains is expected for fields around the symmetrically equivalent [0$\bar{1}$0] and the [100] directions, i.e. for θ around 45^o and -135^o. Instead, we observe an increased magnetoresistance around $\theta = 0^o$ and -180^o. The increase of magnetoresistance along the [$\pm$1 $\pm$1 0] field direction is also not consistent with a change in the density of states mostly along the current direction[18]. The spin-density wave is expected to gap quasiparticles of the Fermi surface along the SDW ordering vector direction $\boldsymbol{k}$, which is always out of the plane normal to the rotation axis (see Supplementary Information I). Despite the ordering vector component along the [001] direction, an increase of the resistivity where $\boldsymbol{J}$ is almost parallel to $\boldsymbol{k}$ would be expected from the gapped Fermi surface along the same direction. Instead, the resistivity enhancement we observe here is maximal when $\boldsymbol{J}$ is mostly perpendicular to $\boldsymbol{k}$.

Therefore, the AFM AMR detected may arise from differences in the transport scattering rates for $\boldsymbol{J} \parallel \boldsymbol{k}$ and $\boldsymbol{J} \perp \boldsymbol{k}$. Notably, a more resistive state is observed for electrons traveling within the stripes along the effective ferromagnetic direction (see Fig.4(a)) and the resistance is lower when the current is along the modulation direction. An enhanced conductivity along the AFM direction also observed in iron arsenides was attributed to a nematic susceptibility[35,36]. In these compounds however, the resistivity anisotropy persists in the non-magnetic regime, while in our case the enhancement is connected to the AFM phase. Multiband scattering rates associated with a large interband spin-orbit coupling in $\mathrm{Nd}_x\mathrm{Ce}_{1-x}\mathrm{CoIn}_5$ give rise to this extraordinary anisotropic magnetoresistance effect, leading to an increased resistivity along the AFM direction. We show that an anisotropic magnetoresistance signal of $\sim 8\%$ related to in-situ switching AFM domains is found in a simple antiferromagnetic resistor without any supplementary layer.

In summary, we demonstrate a general approach for manipulating antiferromagnetic domains without relying on the Zeeman coupling or a coupling of the AFM order with any additional order parameter. We discovered a new AMR effect that is directly related to switching antiferromagnetic k-domains. Notably, we probed sizable differences in transport scattering rates determined by the relative orientation between the electrical current and the antiferromagnetic ordering vector. At a very fundamental level, our results provide a qualitative new route for manipulating and detecting AFM domains without involving the moment orientation at any stage. This route is promising because it provides means for manipulating and detecting AFM states without compromising the robustness offered by antiferromagnets. Moreover, this newly reported phenomenon calls for further theoretical and experimental exploration to gain additional insights into the magnitude of the AFM magnetoresistance signal. Primary candidates for the occurrence of such phenomena are rare-earth multiband materials, where the spin-orbit interaction is known to be enhanced and often of the order of the Fermi energy[2]. In view of the ongoing efforts to unravel novel antiferromagnetic structures, we expect to have broader scope for finding similar effects on other compounds where AFM k-domains form in materials with large spin-orbit coupling.

---

[1] Jungwirth, T., Marti, X., Wadley, P., and Wunderlich, J. 'Antiferromagnetic spintronics'. *Nature nanotechnology* **11**, 231 (2016).

[2] Mineev, V. 'Antiferromagnetic order in $CeCoIn_5$ oriented by spin-orbital coupling'. *Low Temperature Physics* **43**, 11 (2017).

[3] Blundell, S. 'Magnetism in condensed matter' (2003).

[4] Kakehashi, Y. 'Modern Theory of Magnetism in Metals and Alloys'. *Springer Science and Business Media* **175** (2013).

[5] Tanner, B. 'Antiferromagnetic domains'. *Contemporary Physics* **20**, 187 (1979).

[6] Song, C., You, Y., Chen, X., Zhou, X., Wang, Y., and Pan, F. 'How to manipulate magnetic states of antiferromagnets'. *Nanotechnology* **29**, 112001 (2018).

[7] Baltz, V., Manchon, A., Tsoi, M., Moriyama, T., Ono, T., and Tserkovnyak, Y. 'Antiferromagnetic spintronics'. *Rev. Mod. Phys.* **90**, 015005 (2018).

[8] Chappert, C., Fert, A., and Van Dau, F.N. 'The emergence of spin electronics in data storage'.

Nanoscience And Technology: A Collection of Reviews from Nature Journals pages 147–157 (2010).

[9] Kimel, A., Kirilyuk, A., Tsvetkov, A., Pisarev, R., and Rasing, T. 'Laser-induced ultrafast spin reorientation in the antiferromagnet TmFeO 3'. *Nature* **429**, 850 (2004).

[10] Qiu, H., Zhou, L., Zhang, C., Wu, J., Tian, Y., Cheng, S., Mi, S., Zhao, H., Zhang, Q., Wu, D., *et al.* 'Ultrafast spin current generated from an antiferromagnet'. *Nature Physics* **17**, 388 (2021).

[11] Železný, J., Gao, H., Výborný, K., Zemen, J., Mašek, J., Manchon, A., Wunderlich, J., Sinova, J., and Jungwirth, T. 'Relativistic Néel-Order Fields Induced by Electrical Current in Antiferromagnets'. *Phys. Rev. Lett.* **113**, 157201 (2014).

[12] Jungfleisch, M.B., Zhang, W., and Hoffmann, A. 'Perspectives of antiferromagnetic spintronics'. *Physics Letters A* **382**, 865 (2018).

[13] Kampfrath, T., Sell, A., Klatt, G., Pashkin, A., Mährlein, S., Dekorsy, T., Wolf, M., Fiebig, M., Leitenstorfer, A., and Huber, R. 'Coherent terahertz control of antiferromagnetic spin waves'. *Nature Photonics* **5**, 31 (2011).

[14] Arrott, A., Werner, S.A., and Kendrick, H. 'First-Order Magnetic Phase Change in Chromium at 38.5°C'. *Phys. Rev. Lett.* **14**, 1022 (1965).

[15] Werner, S.A., Arrott, A., and Kendrick, H. 'Temperature and Magnetic-Field Dependence of the Antiferromagnetism in Pure Chromium'. *Phys. Rev.* **155**, 528 (1967).

[16] Cheong, S.W., Fiebig, M., Wu, W., Chapon, L., and Kiryukhin, V. 'Seeing is believing: visualization of antiferromagnetic domains'. *npj Quantum Materials* **5**, 1 (2020).

[17] Hedrich, N., Wagner, K., Pylypovskyi, O.V., Shields, B.J., Kosub, T., Sheka, D.D., Makarov, D., and Maletinsky, P. 'Nanoscale mechanics of antiferromagnetic domain walls'. *Nature Physics* **17**, 574 (2021).

[18] Muir, W.B. and Ström-Olsen, J.O. 'Electrical Resistance of Single-Crystal Single-Domain Chromium from 77 to 325 °K'. *Phys. Rev. B* **4**, 988 (1971).

[19] Fawcett, E. 'Spin-density-wave antiferromagnetism in chromium'. *Rev. Mod. Phys.* **60**, 209 (1988).

[20] Shick, A.B., Khmelevskyi, S., Mryasov, O.N., Wunderlich, J., and gwirth, T. 'Spin-orbit coupling induced anisotropy effects in bimetallic antiferromagnets: A route towards antiferromagnetic spintronics'. *Phys. Rev. B* **81**, 212409 (2010).

[21] Jungwirth, T., Novák, V., Martí, X., Cukr, M., Máca, F., Shick, A.B., Mašek, J., Horodyská, P., Němec, P., Holý, V., Zemek, J., Kužel, P., Němec, I., Gallagher, B.L., Campion, R.P., Foxon, C.T., and Wunderlich, J. 'Demonstration of molecular beam epitaxy and a semiconducting band structure for I-Mn-V compounds'. *Phys. Rev. B* **83**, 035321 (2011).

[22] Železnỳ, J., Wadley, P., Olejník, K., Hoffmann, A., and Ohno, H. 'Spin transport and spin torque in antiferromagnetic devices'. *Nature Physics* **14**, 220 (2018).

[23] Fåk, B., Adroja, D.T., Enderle, M., Böhm, M., Lapertot, G., and Mineev, V.P. 'Anomalous spin response in the non-centrosymmetric metal $CePt_3Si$'. *Journal of the Physical Society of Japan* **83**, 063703 (2014).

[24] Feng, Y., Jiang, Q., Feng, B., Yang, M., Xu, T., Liu, W., Yang, X., Arita, M., Schwier, E.F., Shimada, K., *et al.* 'Rashba-like spin splitting along three momentum directions in trigonal layered $PtBi_2$'. *Nature communications* **10**, 1 (2019).

[25] Takimoto, T. 'Anomalous Spin Response in Non-centrosymmetric Compounds'. *Journal of the Physical Society of Japan* **77**, 113706 (2008).

[26] Hu, R., Lee, Y., Hudis, J., Mitrovic, V.F., and Petrovic, C. 'Composition and field-tuned magnetism and superconductivity in $Nd_{1-x}Ce_xCoIn_5$'. *Phys. Rev. B* **77**, 165129 (2008).

[27] Mazzone, D.G., Gauthier, N., Maimone, D.T., Yadav, R., Bartkowiak, M., Gavilano, J.L., Raymond, S., Pomjakushin, V., Casati, N., Revay, Z., Lapertot, G., Sibille, R., and Kenzelmann, M. 'Evolution of Magnetic Order from the Localized to the Itinerant Limit'. *Phys. Rev. Lett.* **123**, 097201 (2019).

[28] Klotz, J., Götze, K., Sheikin, I., Förster, T., Graf, D., Park, J.H., Choi, E.S., Hu, R., Petrovic, C., Wosnitza, J., and Green, E.L. 'Fermi surface reconstruction and dimensional topology change in Nd-doped $CeCoIn_5$'. *Phys. Rev. B* **98**, 081105 (2018).

[29] Gerber, S., Bartkowiak, M., Gavilano, J.L., Ressouche, E., Egetenmeyer, N., Niedermayer, C., Bianchi, A.D., Movshovich, R., Bauer, E.D., Thompson, J.D., *et al.* 'Switching of magnetic domains reveals spatially inhomogeneous superconductivity'. *Nature Physics* **10**, 126 (2014).

[30] Hatakeyama, Y. and Ikeda, R. 'Antiferromagnetic order oriented by Fulde-Ferrell-Larkin-Ovchinnikov superconducting order'. *Physical Review B* **91**, 094504 (2015).

[31] Maimone, D.T. *Intertwined ordered states in $Nd_xCe_{1-x}CoIn_5$*. PhD thesis, University of Basel and Paul Scherrer Institut (2021).

[32] Wang, H., Lu, C., Chen, J., Liu, Y., Yuan, S.L., Cheong, S.W., Dong, S., and Liu, J.M. 'Giant anisotropic magnetoresistance and nonvolatile memory in canted antiferromagnet Sr_2IrO_4'. *Nature communications* **10**, 1 (2019).

[33] Fundamentals, M. 'E. du Tremolet de Lacheisserie, D. Gignoux and M. Schlenker' (2003).

[34] Putley, E.H. and Landwehr, G. 'The Hall Effect and Related Phenomena'. *Journal of The Electrochemical Society* **109**, 42C (1962).

[35] Chu, J.H., Analytis, J.G., De Greve, K., McMahon, P.L., Islam, Z., Yamamoto, Y., and Fisher, I.R. 'In-plane resistivity anisotropy in an underdoped iron arsenide superconductor'. *Science* **329**, 824 (2010).

[36] Lu, X., Park, J., Zhang, R., Luo, H., Nevidomskyy, A.H., Si, Q., and Dai, P. 'Nematic spin correlations in the tetragonal state of uniaxial-strained BaFe2- xNixAs2'. *Science* **345**, 657 (2014).

[37] Petrovic, C., Pagliuso, P., Hundley, M., Movshovich, R., Sarrao, J., Thompson, J., Fisk, Z., and Monthoux, P. 'Heavy-fermion superconductivity in CeCoIn5 at 2.3 K'. *Journal of Physics: Condensed Matter* **13**, L337 (2001).

I. METHODS

Samples. Single crystals of Nd doped $CeCoIn_5$ were grown in an In self-flux as described elsewhere[27,37].

Resistivity measurements. Electrical properties of $Nd_{0.1}Ce_{0.9}CoIn_5$ were investigated by resistivity measurements conducted in an 11T horizontal magnet from Oxford instruments. In a horizontal magnet, a rotation of the dilution stick is a rotation of the sample orientation with respect to the magnetic field. The single-crystal was mounted in a way such that the magnetic field was rotated about the c-axis. The sample was aligned by Laue X-ray diffraction and cut in a thin piece of dimensions 1.2 mm $\times$ 0.4 mm $\times$ 0.1 mm. The electrical current of magnitude 10^3 Ampere per square meter was applied almost parallel to the crystallographic [110] direction. To apply current to the sample, we equipped the dilution unit with superconducting NbTi in CuNi-matrix wires order to reduce the heat load. Between the mixing chamber and the sample we use NbTi in a Cu-matrix. The sample was attached to a copper holder on a copper cold finger to position the sample in the center of the magnet. The Cu-matrix ensured good thermalization to the mixing chamber. In fact, sample cooling is mainly provided by the current leads as the main thermal path. The sample was mounted in a conventional four-wire configuration with current contacts soldered onto the crystal edges. This reduced the contact resistance to $\approx 1\ \Omega$ and minimized the Joule heating. The voltage contacts were glued onto the sample with silver epoxy.

The superconducting phase diagram of $Nd_{0.17}Ce_{0.83}CoIn_5$ and the absence of superconductivity in $Nd_{0.25}Ce_{0.75}CoIn_5$ was obtained from resistivity measurements performed in a similar fashion to what was done for $Nd_{0.1}Ce_{0.9}CoIn_5$, but with electrical currents applied along the [100] and fields applied along the [010] direction. For these measurements, we used a vertical 15T cryomagnet from Oxford Instruments.

High field neutron diffraction experiments. Experiments on $Nd_{0.1}Ce_{0.9}CoIn_5$ and $Nd_{0.17}Ce_{0.83}CoIn_5$ were carried out on Rita-II triple-axis spectrometer and Zebra diffractometer at the Paul Scherrer Institut, Villigen, Switzerland. Experiments on $Nd_{0.25}Ce_{0.75}CoIn_5$ were performed on D23 diffractometer at the Institut Laue-Langevin, in Grenoble, France. Low temperatures below 50 mK and high magnetic fields up to $\mu_0 H = 15$ T were reached using a dilution insert inside the cryomagnets. The single-crystals were aligned in the [h, h, l] plane in reciprocal space and exposed to $\lambda = 1.28\mathring{A}$ for Zebra and D23, and $4.217\mathring{A}$ for Rita-II. The analyzer unit of Rita-II lowers the background, providing an advantage for our experiments where we deal with small ordered moments. However, high magnetic field experiments limit the access of diffraction peaks to a particular reciprocal lattice plane, as tilting the cryomagnet cannot be done. In order to perform measurements out of the horizontal scattering plane, the diffractometers Zebra and D23 have lifting arm detectors, thus enabling measurements of the two magnetic domains $\boldsymbol{k}^{+,-}$ in a single experiment. For these measurements, we used 10 T vertical magnet. This was due to the fact that the 15 T has a small vertical opening of $\pm\ 2^o$, making it impossible to measure the magnetic domain $\mathbf{k}^-$ which is out of scattering plane for samples aligned in the [h,h,l] horizontal scattering plane.

The magnetic phase diagrams shown in Fig.2 were obtained from field and temperature dependences from position-optimized counts on top of the magnetic peaks $(q, \pm q, 0.5)$. For $Nd_{0.1}Ce_{0.9}CoIn_5$, the phase boundaries were obtained from field scans at $T = 0.08, 0.7$ and 1K and temperature scans at $\mu_0 H = 0, 4, 8, 12$T. For $Nd_{0.17}Ce_{0.83}CoIn_5$, the mapping of the HT-phase diagram was performed with field scans at $T = 0.18, 0.5$ and 0.8K and temperature scans at $\mu_0 H = 2, 4, 6, 7, 9$ and 12.5T.

II. ACKNOWLEDGEMENTS

We acknowledge the Paul Scherrer Institut (Villigen, Switzerland) and the Institut Laue-Langevin (Grenoble, France) for the allocated beamtime. We acknowledge funding from the Swiss National Science Foundation (grant 200021_162671) and the Swiss State Secretariat for Education, Research and Innovation (SERI) through the CRG grants (CRG-2460 and CRG-2639).

III. AUTHOR CONTRIBUTIONS

D.T.M., M.B., and M.K. planned and led the study. The samples were grown by D.T.M., J.S., R.Y., N.G., D.G.M, D.J.G., E.P. and G.L.. Neutron diffraction experiments were performed by D.T.M., N.G., J.S., D.G.M., R.Y., J.L.G., M.B., M.K., with C.N., R.S., S.R., E.R. as instrument scientists. Sample preparation for the neutron diffraction and resistivity measurements was realized by D.T.M.. Resistivity measurements were carried out by D.T.M., with the assistance from M.Z., M.B. and M.K.. D.T.M. analyzed the data. D.T.M., N.G., D.G.M., S.R., M.B. and M.K. discussed the interpretation of the results. The manuscript was written by D.T.M. in close collaboration with M.B. and M.K. and with feedback from all coauthors.

IV. COMPETING INTERESTS

The authors declare no competing interests.

V. ADDITIONAL INFORMATION

Supplementary Information is available for this paper.

Correspondence and requests for materials should be addressed to D.T.M..

Supplementary Files

This is a list of supplementary files associated with this preprint. Click to download.

- supplSOCAFMdomainsnoZeeman.pdf